Polysaccharide elasticity governed by chair–boat transitions of the glucopyranose ring

Piotr E. Marszalek*, Andres F. Oberhauser*, Yuan-Ping Pang† & Julio M. Fernandez*

** Department of Physiology and Biophysics, † Mayo Clinic Cancer Center and Department of Pharmacology, Mayo Foundation, Rochester, Minnesota 55905, USA*

Many common, biologically important polysaccharides contain pyranose rings made of five carbon atoms and one oxygen atom. They occur in a variety of cellular structures, where they are often subjected to considerable tensile stress[1–6]. The polysaccharides are thought to respond to this stress by elastic deformation, but the underlying molecular rearrangements allowing such a response remain poorly understood. It is typically assumed, however, that the pyranose ring structure is inelastic and locked into a chair-like conformation. Here we describe single-molecule force measurements[7–12] on individual polysaccharides that identify the pyranose rings as the structural unit controlling the molecule's elasticity. In particular, we find that the enthalpic component of the polymer elasticity[10,11,13,14] of amylose, dextran and pullulan is eliminated once their pyranose rings are cleaved. We interpret these observations as indicating that the elasticity of the three polysaccharides results from a force-induced elongation of the ring structure and a final transition from a chair-like to a boat-like conformation. We expect that the force-induced deformation of pyranose rings reported here plays an important role in accommodating mechanical stresses and modulating ligand binding in biological systems.

Polymeric molecules based on the pyranose ring form a wide variety of polysaccharides that receive different names depending on the type of the monomer(s) and the glycosidic linkages. X-ray crystallography and neutron diffraction have shown that the most stable conformation of the pyranose ring structures is the chair $^4C_1$ conformer[15–17]. Molecular dynamics simulations have confirmed that the chair $^4C_1$ conformer is the most populated structure: these simulations also suggested that the ring structure in the chair conformation is flexible because a range of chair distortions are allowed without significant changes in the conformational energy[18–20].

Some of these polysaccharides can be oxidized by periodate under mild conditions. The reaction is highly specific and results in the cleavage of the ring structure to form an acyclic backbone with intact glycosidic linkages[21]. We have found that such ring cleavage removes the enthalpic component of the elasticity of the three polysaccharides we have studied, demonstrating the central role played by the pyranose ring in polysaccharide elasticity. Figure 1 shows the effect, over time, of mild periodate oxidation on the elasticity of single dextran (Fig. 1a), amylose (Fig. 1b) and pullulan (Fig. 1c) molecules.

The dextran molecule is a polymer formed by glycosidic bonds linking the carbon atoms number 1 and 6 of consecutive α-D-glucopyranose rings (Fig. 1a inset). As previously shown by Rief *et al.*[10], dextran molecules have a large enthalpic component in their elasticity that is evident as a prolonged plateau in the force–extension curve (Fig. 1a, black trace). The dextran monomer has two sites that are cleaved by periodate oxidation (2–3 and 3–4; Fig. 1a, red arrows in inset). As the figure shows, periodate oxidation causes a gradual disappearance of the enthalpic elasticity. The elasticity of polymers such as dextran has been shown to be well described by a modified 'freely jointed chain' (FJC) model that predicts the relationship between the extension of the polymer and the entropic restoring force generated[10,13,22]. The adjustable parameters of the FJC model are the contour length of the polymer, l_c, the Kuhn (segment) length, l_K, and the elasticity of each individual segment, S_e. Fits of the FJC function to the force–extension curves obtained for the polysaccharides adequately described their elasticity (thin lines, Fig. 1). The changes in the elasticity of the dextran molecule during periodate oxidation can be followed by using the FJC model. In the low-force regime, the native dextran molecule is well described by the FJC model with a Kuhn length of $l_K = 0.44$ nm (corresponding to the size of a monomer; see Table 1), and segment elasticity $S_e = 14{,}600 \pm 2{,}700$ pN nm^{-1} ($n = 23$). However, after periodate oxidation the Kuhn length becomes smaller, $l_K = 0.2 \pm 0.026$ nm ($n = 13$), and the segments become less extensible ($S_e = 34{,}200 \pm 8{,}300$ pN nm^{-1}, $n = 13$).

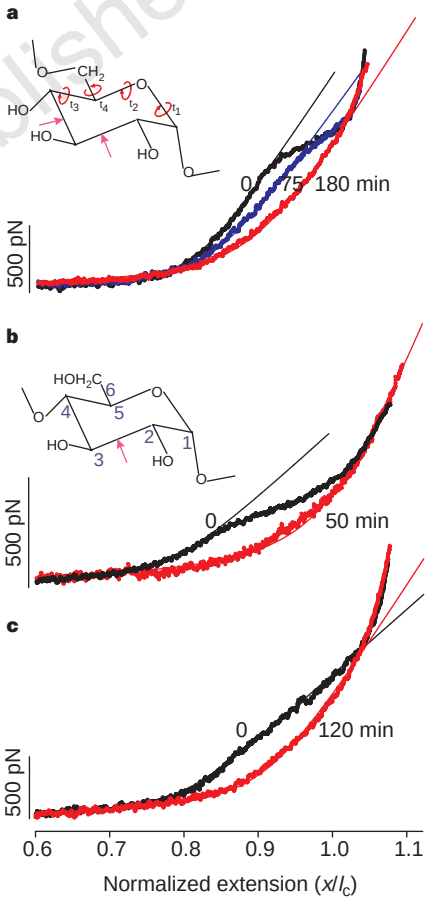

Figure 1 Force–extension curves for single polysaccharide molecules. These curves show that cleavage of the pyranose ring by mild periodate oxidation nearly eliminates the enthalpic component of the elasticity of these polymers. The insets in **a** and **b** show the chemical structure of the monomers of dextran and amylose, respectively. The red arrows mark the cleavage sites. t_1–t_4 represent the ring torsion angles. Oxidation with 5 mM periodate for up to 180 min eliminated the plateau region of the force–extension curves of dextran (**a**), amylose (**b**) and pullulan (**c**) and altered their elasticity such that their force–extension curves approached those of a chain made of rigid elements. In all cases, the extension, x, was normalized by the contour length for each molecule, l_c. To monitor the changes in elasticity during oxidation, we fitted the experimental force–extension curves with the FJC model (thin lines). The FJC fits show that periodate oxidation reduced the Kuhn segment length and increased the stiffness of the segments (see text for details). These results demonstrate that the pyranose ring is the principal extensible element of these polysaccharides.

A large enthalpic elasticity is also observed in amylose, an α-(1 → 4) D-glucopyranose polymer (Fig. 1b). However, the plateau observed in the force–extension curve for amylose has a much lower force threshold (275 ± 45 pN; $n = 11$) than that observed for dextran (850 ± 140 pN; $n = 23$). The amylose monomer has only one site that is cleaved by periodate oxidation, breaking the structure of the pyranose ring (2–3; Fig. 1b, red arrow in inset). The polysaccharide pullulan is another polymer of glucose combining the α-(1 → 4) and α-(1 → 6) glycosidic linkages (2:1 ratio) which also shows a pronounced enthalpic elasticity that appears to result from a combination of those observed for dextran and amylose (Fig. 1c). The pullulan monomers contain the combined cleavage sites of both dextran and amylose (not shown).

Similar to the results with dextran, periodate oxidation eliminated the enthalpic component of the chain elasticity of amylose and pullulan (Fig. 1b, c) and made their segments more rigid. Cleavage of the amylose ring reduced the length of the Kuhn segment from 0.45 nm (Table 1) to 0.18 ± 0.025 nm ($n = 12$) and increased segment elasticity (from $S_e = 5{,}600 \pm 800$ pN nm^{-1} to 34,000 ± 7,300 pN nm^{-1}; $n = 12$). Cleavage of the rings in pullulan reduced the length of the Kuhn segment from 0.45 nm to 0.2 ± 0.015 nm ($n = 6$) and increased their segment elasticity (from $S_e = 10{,}200 \pm 930$ pN nm^{-1} to 47,800 ± 5,000 pN nm^{-1}; $n = 6$). In all cases, periodate oxidation alters the chain segments such that they become shorter and stiffer.

The force–extension curves of dextran, amylose and pullulan are all significantly different, and seem to depend on the attachment points of the glycosidic bond to the glucopyranose ring (Fig. 1). However, cleavage of the pyranose ring converts the elastic behaviour of these polysaccharides into a simple entropic spring which is similar for all three molecules (Fig. 2).

We note that the force–extension curves reported here for amylose and pullulan are fully reversible and show a complete lack of hysteresis, similar to what was observed earlier for dextran[10]. This indicates that the enthalpic elasticity arises from the conformation of the monomers rather than from breaking secondary structure, as was proposed for the elasticity of DNA and xanthan, molecules that show large hysteresis during extension–contraction cycles[13,23].

A prominent characteristic of the enthalpic elasticity of amylose and dextran is a plateau region in the force–extension curve that indicates that the molecule elongates at approximately constant force. Our data show that this elongation must originate from the ring structure. Indeed, a six-membered ring structure can acquire several conformations: chair, boat, twist and half-twist[24]. The glucopyranose ring is typically in the chair ($^4C_1$) conformation. The free energy of interconversion between conformations ranges up to 12 kcal mol^{-1} for the free monomers in solution[25]. The distance between two consecutive glycosidic oxygens (a residue vector, $\mathbf{O}_i\mathbf{O}_j$) —which determines the length of the monomer in a polysaccharide chain—is expected to vary with the pyranose ring conformation. (This is evident on inspection of a simple ball-and-stick model of the pyranose; Fig. 3a.) Stretching the polysaccharide chain with an external force is likely to favour conformations of the ring that provide a greater separation of the glycosidic oxygens, as this will lead to an extension of the molecule. In order to verify this view, we have made *ab initio* calculations of the length of the residue vector $\mathbf{O}_i\mathbf{O}_j$ in all thermodynamically accessible conformations—including the chair and boat conformations of the pyranose ring for amylose and dextran (Table 1). For these molecules, the transition from chair to boat conformation increases the length of the $\mathbf{O}_i\mathbf{O}_j$ initio calculations of the extension of the $\mathbf{O}_i\mathbf{O}_j$ vector during the chair–boat transition for amylose (16.2%) and dextran (22.5%) closely match the experimental observations (Table 1; Fig. 3b).

Cellulose is a glucopyranose polymer identical to amylose except

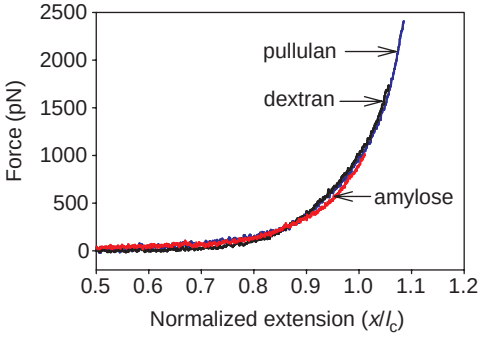

Figure 2 On cleavage of the pyranose ring, single molecules of amylose, pullulan and dextran display identical elastic behaviour. Ring cleavage converts these different polysaccharide chains into similar structures where all the bonds of the polymer backbone, including those that were components of the closed ring structure, can rotate and align under force, contributing equally to the (mainly) entropic elasticity of the chain.

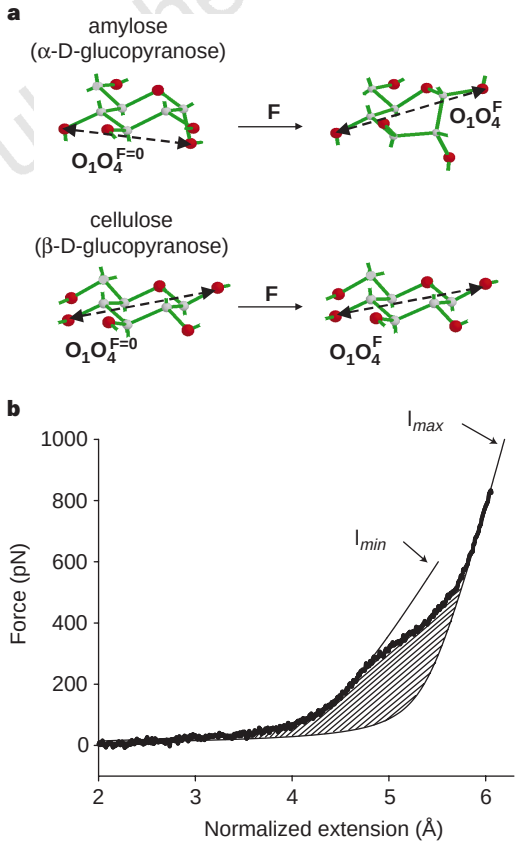

Figure 3 Increased separation of glycosidic oxygen atoms during chair–boat transitions of the glucopyranose ring explains the extensibility of amylose. **a**, The diagrams show that the distance between two consecutive glycosidic oxygens O_1–O_4 increases during a force-driven chair–boat transition when the glycosidic oxygen O_1 is in the axial position (amylose). Buy contrast, the O_1–O_4 distance is already at a maximum when O_1 is in the equatorial position (cellulose). *Ab initio* calculations of the separation of glycosidic oxygen atoms during chair–boat transitions (Table 1) accurately predict the extensibility of amylose, dextran and cellulose. **b**, A force–extension curve for amylose (thick trace) was fitted with the FJC model using a Kuhn length of 4.533 Å before the plateau and a Kuhn length of 5.408 Å after the plateau region (see Table 1). The computed fractional increase in contour length for this recording was 18%. The figure shows the data after normalization by $(O_1\text{–}O_4)/l_c$. The hatched area corresponds to the change in ΔG per monomer to convert it from the chair to the boat conformation. The free energy, ΔG, was determined to be 4.6 kcal mol^{-1} (range 2.5–4.8 kcal mol^{-1}, $n = 11$). Similar measurements made with single dextran molecules showed a ΔG of ~11 kcal mol^{-1}.

Nature © Macmillan Publishers Ltd 1998

that it has an equatorial glycosidic bond to the pyranose ring ($\beta-(1\rightarrow4)$ linkages). *Ab initio* calculations of the $\mathbf{O_1O_4}$ vector for cellulose show that the length of this vector is already at a maximum in the chair conformation (Fig. 3a; Table 1). A transition to the boat and other conformations would decrease the O_1–O_4 distance and is therefore prohibited in the molecule under a stretching force. Hence, these calculations predict that the cellulose molecule should behave as an entropic spring without showing the plateau region which characterizes the conformational transition of the ring structure. Indeed, recordings of the force–extension relationship for carboxymethylated cellulose (made using an atomic force microscope, AFM) do not show a measurable enthalpic component[23]. Similarly, the force–extension relationship for methylcellulose, another soluble derivative of cellulose, does not have a measurable enthalpic component (not shown). These observations are consistent with the known rigidity of cellulose.

We have demonstrated two components of enthalpic elasticity in polysaccharides: under an applied force we observed a continuous elastic deformation of the pyranose ring (for example, 0–200 pN for amylose) and a transitional component (>200 pN). This latter component occurs when the pyranose ring adopts extended conformations that are normally less populated due to their higher conformational energies (chair–boat transition; Fig. 3a). The range of forces required to trigger these conformational changes are found in cellular systems, such as the bacterial and plant cell walls that must accommodate the high tensile stress generated by changes in turgor pressure[5,6]. For example, we have found that pectin, a pyranose-based polysaccharide (an $\alpha-(1\rightarrow4)$ D-galactouronan) and one of the main components of the plant cell wall, has a large enthalpic elasticity, similar to that of amylose. Single pectin molecules undergo an abrupt extension by 18% ($n = 7$) of their length at forces bigger than 200 pN (not shown). Hence, the structural assembly of different types of polysaccharides such as pectins and cellulose may allow plant cells to finely control the extensibility of their cell wall.

Hydroxyl and other functional groups attached to the pyranose ring coordinate the binding of lectins[26]. It is interesting to consider that the force-induced ring deformations demonstrated here may alter the reactivity of the pyranose ring, allowing or preventing the binding of ligands.

Much of the recent progress in understanding the dynamics of biological molecules, a central focus of modern biology, comes from the manipulation of single molecules. The direct mechanical manipulation of a pyranose ring, as demonstrated here, gives a unique and unusual way to control ring conformations which are conventionally governed by the nature of the substituents attached to the rings. As demonstrated by Barton[27], conformational analysis of ring-based substrate and ligands such as steroids provided the elements needed to understand their biological action[27]. Here, we expand the boundaries of conformational analysis by including force-driven changes in ring structure as important, but hitherto unrecognized, biological events. □

Table 1 *Ab initio* calculation of the separation of glycosidic oxygen atoms during chair–boat transitions

	Calculated				Experimental
	O_i–$O_j^{F=0}$ (Å)	O_i–O_j^F (Å)	Δ (Å)	$\frac{\Delta}{O_i\text{–}O_j^F}$ (%)	$\frac{l_{max}-l_{min}}{l_{max}}$ (%)
$Amylose_{\alpha-1,4}$	4.533	5.408	0.875	16.2	16.8 ± 1.8 ($n = 11$)
$Dextran_{\alpha-1,6}$	4.412	5.696	1.284	22.5	19.5 ± 2.1 ($n = 23$)
$Cellulose_{\beta-1,4}$	5.417	5.417	0	0	0 ($n = 29$)

This table compares the distance between glycosidic oxygen atoms, in the relaxed ($F = 0$) and stretched conformations, $(O_i\text{–}O_j^F - O_i\text{–}O_j^{F=0})/O_i\text{–}O_j^F$, with the experimentally measured extension of the contour length, $(l_{max} - l_{min})/l_{max}$. The experimental values for l_{min} and l_{max} were obtained from the fits of the FJC model to the force–extension curve before and after the plateau region (thin lines in Fig. 3b).

Methods

Single-molecule atomic force microscopy. Our custom-made AFM apparatus, as well as its mode of operation, have been described elsewhere[12]: it is capable of measuring individual molecules. The spring constant of each individual AFM tip was calibrated in solution, using the equipartition theorem as described by Florin *et al.*[28]. This method gives values for the spring constant of the cantilever which are within 20% of the values obtained by other methods[28]. The polysaccharides used—dextran T500 (Pharmacia Biotech); amylose (type III: from potato; Sigma); pullulan (from *Aureobasidium pullulans*; Sigma) and methylcellulose (Sigma)—are linear or >95% linear (dextran) homopolymers of D-glucopyranose (relative molecular mass $M_r > 10^5$). Dextran has short branches which frequently consist of just a single glucose at the position 3. Pectin (from citrus fruits; Sigma) is an $\alpha-(1\rightarrow4)$ D-galactouronan. Dextran, pullulan, methylcellulose and pectin were dissolved in water at a concentration of 0.1–10% (w/v). Amylose was solubilized by wetting with ethanol (100 mg ml^{-1}), followed by treatment with sodium hydroxide solution (10%) and heating. The final concentration of amylose was 0.2–1% (w/v). A layer of polysaccharide molecules was created by drying a drop of these solutions onto glass coverslips followed by extensive rinsing. This procedure leaves a monolayer of polysaccharide molecules tightly adsorbed to the glass surface[23]. The measurements were carried out in water or in PBS buffer (pectin). For ring cleavage, the polysaccharide samples were treated with 5 mM sodium meta-periodate (Sigma) for up to 180 min. To pick polysaccharide molecules, an AFM tip was pressed down onto the sample for 1–3 s at forces of several nanonewtons. A subsequent force–extension measurement typically revealed a complex pattern with many overlapping force peaks. By manipulating the polysaccharide concentration and the force and duration of the tip–sample contact, it was possible to regularly obtain single polysaccharide force–extension curves.

***Ab initio* calculation of the glucopyranose ring conformations.** Different conformations of the glucopyranose ring were generated by specifying all discrete possibilities at increments of 60 degrees of arc in the range 0–360° for torsions t_1–t_4 (Fig. 1a). These conformers were optimized first with molecular mechanics calculation (Quanta97/CHARMm)[29] and then with *ab initio* calculation (GAUSSIAN94, HF/6-31G*//HG/6-31G*)[30]. The length of the residue vector in the relaxed state of a polysaccharide (no external force) was obtained from the distance between the two consecutive glycosidic oxygen atoms (O_i–O_j) in the most stable glucopyranose conformer (chair). The corresponding length of the residue vector in the stretched polysaccharide was obtained from the maximal O_i–O_j distance found in all the conformers optimized by the *ab initio* calculation. The separations of the glycosidic oxygen atoms O_i–O_j in the conformations representing the relaxed ($F = 0$) and stretched states of the glucopyranose monomers in amylose, dextran, and cellulose are shown in Table 1. For amylose and dextran, these maximal distances corresponded to the boat conformation. For cellulose, the O_i–O_j distance is already maximal in the chair conformation indicating that an external force will not trigger a chair–boat transition.

Received 18 September; accepted 25 November 1998.

1. McEver, R. P., Moore, K. L. & Cummings, R. D. Leukocyte trafficking mediated by selective carbohydrate interactions. *J. Biol. Chem.* **270,** 11025–11028 (1995).
2. Rosen, S. D. & Bertozzi, C. R. Leukocyte adhesion: two selectins converge on sulphate. *Curr. Biol.* **6,** 261–264 (1996).
3. Alon, R., Hammer, D. A. & Springer, T. A. Lifetime of the P-selectin-carbohydrate bond and its response to tensile force in hydrodynamic flow. *Nature* **374,** 539–542 (1995).
4. Puri, K. D., Chen, S. & Springer, T. A. Modifying the mechanical property and shear threshold of L-selectin adhesion independently of equilibrium properties. *Nature* **392,** 930–933 (1998).
5. Cosgrove, D. J. Relaxation in a high-stress environment: the molecular bases of extensible cell walls and cell enlargement. *Plant Cell* **9,** 1031–1041 (1997).
6. Thwaites, J. J. & Mendelson, N. H. Biomechanics of bacterial walls: studies of bacterial thread made from Bacillus subtilis. *Proc. Natl Acad. Sci. USA* **82,** 2163–2167 (1985).
7. Bustamante, C., Rivetti, C. & Keller, D. J. Scanning force microscopy under aqueous solutions. *Curr. Opin. Struct. Biol.* **7,** 709–716 (1997).
8. Florin, E. L., Moy, V. T. & Gaub, H. E. Adhesion forces between individual ligand-receptor pairs. *Science* **264,** 415–417 (1994).
9. Lee, G. U., Chrisey, L. A. & Colton, R. J. Direct measurement of the forces between complementary strands of DNA. *Science* **266,** 771–773 (1994).
10. Rief, M., Oesterhelt, F., Heymann, B. & Gaub, H. E. Single molecule force spectroscopy on polysaccharides by atomic force microscopy. *Science* **275,** 1295–1297 (1997).
11. Rief, M., Gautel, M., Oesterhelt, F., Fernandez, J. M. & Gaub, H. E. Reversible unfolding of individual titin immunoglobulin domains by AFM. *Science* **276,** 1109–1112 (1997).
12. Oberhauser, A. F., Marszalek, P. E., Erickson, H. P. & Fernandez, J. M. The molecular elasticity of the extracellular matrix protein tenascin. *Nature* **393,** 181–185 (1998).

13. Smith, S. B., Cui, Y. & Bustamante, C. Overstretching B-DNA: the elastic response of individual double-stranded and single-stranded DNA molecules. *Science* **271,** 795–799 (1996).
14. Rief, M., Fernandez, J. M. & Gaub, H. E. Elastically coupled two-level-systems as a model for biopolymer extensibility. *Phys. Rev. Lett.* **81,** 4764–4767 (1998).
15. Brown, G. M. & Levy, H. A. α-D-Glucose: precise determination of crystal and molecular structure by neutron-diffraction analysis. *Science* **147,** 1038–1039 (1965).
16. Chu, S. C. C. & Jeffrey, G. A. The refinement of the crystal structures of β-D-glucose and cellobiose. *Acta. Crystallogr. B* **24,** 830–838 (1968).
17. Brown, G. M. & Levy, H. A. α-D-Glucose: further refinement based on neutron-diffraction data. *Acta Crystallogr. B* **35,** 656–659 (1979).
18. Brady, J. W. Molecular dynamics simulations of α-D-glucose. *J. Am. Chem. Soc.* **108,** 8153–8160 (1986).
19. Brady, J. W. Molecular dynamics simulations of β-D-glucopyranose. *Carbohydr. Res.* **165,** 306–312 (1987).
20. Joshi, N. V. & Rao, V. S. R. Flexibility of the pyranose ring in α- and β-D-glucoses. *Biopolymers* **18,** 2993–3004 (1979).
21. Bobbitt, J. M. in *Advances in Carbohydrate Chemistry* (eds Wolfram, M. L. & Tipson, R. S.) 1–4 (Academic, New York, 1956).
22. Smith, S. B., Finzi, L. & Bustamante, C. Direct mechanical measurements of the elasticity of single DNA molecules by using magnetic beads. *Science* **258,** 1122–1126 (1992).
23. Li, H., Rief, M., Oesterhelt, F. & Gaub, H. E. Single-molecular force spectroscopy on xanthan by AFM. *Adv. Mater.* **3,** 316–319 (1998).
24. Kellie, G. M. & Riddell, F. G. Non-chair conformations of six-membered rings. *Top. Stereochem.* **8,** 225–264 (1974).
25. Pickett, H. M. & Strauss, H. L. Conformational structure, energy, and inversion rates of cyclohexane and some related oxanes. *J. Am. Chem. Soc.* **92,** 7281–7290 (1970).
26. Drickamer, K. Making a fitting choice: common aspects of sugar-binding sites in plant and animal lectins. *Structure* **5,** 465–468 (1997).
27. Barton, D. H. R. The principles of conformational analysis. *Science* **169,** 539–544 (1970).
28. Florin, E. L. *et al*. Sensing specific molecular interactions with the atomic force microscope. *Biosensors Bioelectr.* **10,** 895–901 (1995).
29. Quanta97/CHARMm (Molecular Simulations, 9685 Scranton Rd, San Diego, California 92121, USA, 1997).
30. Gaussian 94 (Gaussian Inc., Carnegie Office Prk, Bldg 6, Pittsburgh, Pennsylvania 15106, USA, 1994).

Acknowledgements. This work was supported by the NSF (P.E.M.) and the NIH (J.M.F.).

Correspondence and requests for materials should be addressed to J.M.F. (e-mail: fernandez.julio@mayo.edu).

Effect of interannual climate variability on carbon storage in Amazonian ecosystems

Hanqin Tian*, Jerry M. Melillo*, David W. Kicklighter*, A. David McGuire†, John V. K. Helfrich III*, Berrien Moore III‡ & Charles J. Vörösmarty‡

** The Ecosystems Center, Marine Biological Laboratory, Woods Hole, Massachusetts 02543, USA*
† US Geological Survey, Alaska Cooperative Fish and Wildlife Research Unit, University of Alaska, Fairbanks, Alaska 99775, USA
‡ Institute for the Study of Earth, Oceans and Space, University of New Hampshire, New Hampshire 03824, USA

The Amazon Basin contains almost one-half of the world's undisturbed tropical evergreen forest as well as large areas of tropical savanna[1,2]. The forests account for about 10 per cent of the world's terrestrial primary productivity and for a similar fraction of the carbon stored in land ecosystems[2,3], and short-term field measurements[4] suggest that these ecosystems are globally important carbon sinks. But tropical land ecosystems have experienced substantial interannual climate variability owing to frequent El Niño episodes in recent decades[5]. Of particular importance to climate change policy is how such climate variations, coupled with increases in atmospheric CO_2 concentration, affect terrestrial carbon storage[6–8]. Previous model analyses have demonstrated the importance of temperature in controlling carbon storage[9,10]. Here we use a transient process-based biogeochemical model of terrestrial ecosystems[3,11] to investigate interannual variations of carbon storage in undisturbed Amazonian ecosystems in response to climate variability and increasing atmospheric CO_2 concentration during the period 1980 to 1994. In El Niño years, which bring hot, dry weather to much of the Amazon region, the ecosystems act as a source of carbon to the atmosphere (up to 0.2 petagrams of carbon in 1987 and 1992). In other years, these ecosystems act as a carbon sink (up to 0.7 Pg C in 1981 and 1993). These fluxes are large; they compare to a 0.3 Pg C per year source to the atmosphere associated with deforestation in the Amazon Basin in the early 1990s[12]. Soil moisture, which is affected by both precipitation and temperature, and which affects both plant and soil processes, appears to be an important control on carbon storage.

Carbon fluxes calculated using the Terrestrial Ecosystem Model (TEM) include net primary production (NPP), microbial respiration (R_H) and net ecosystem production (NEP), all of which are influenced by climate. Net primary production, the net amount of carbon captured by plants, is also influenced by atmospheric CO_2 concentration. The difference between NPP and R_H equals NEP, which is equivalent to annual net carbon storage or loss for an ecosystem.

For regional or global extrapolations with TEM, we use input data on vegetation, elevation, soil texture, monthly mean temperature, monthly mean precipitation, and monthly mean solar radiation. The input data sets are gridded at a resolution of 0.5° latitude by 0.5° longitude. The structure, parametrization, calibration and performance of TEM have been documented previously[3,11].

We first ran TEM in equilibrium mode to generate an initial condition for the transient runs, using the long-term mean of monthly temperature, monthly precipitation, monthly solar radiation and the level of atmospheric CO_2 concentration at the beginning of this century (296 p.p.m.y.). Then we ran TEM in transient mode using historical input data from 1900 to 1994 including: (1) historical mean atmospheric CO_2 concentration generated from atmospheric and ice core CO_2 observations[13], and (2) historical monthly data for air temperature[14] and precipitation[15]. The historical temperature and precipitation data were interpolated by the Max Planck Institute for Meteorology to a 0.5° spatial resolution. Two transient runs were made: one considering the climate and CO_2 transients together, and one considering only the climate transient. A comparison of these two runs was used to determine the effect of CO_2 'fertilization' on carbon storage. All other model analyses were based on the combined climate and CO_2 transient run. We used the IGBP-DIS land-cover data set[16] as a basis for adjusting the area of undisturbed ecosystems in the Basin to account for land-cover conversions such as forest to cropland. This reduces the area of undisturbed ecosystems by 11%, which is in good agreement with other land-cover change estimates for the Basin[12,17].

For the Amazon Basin, TEM results (Table 1) show that annual NEP varied from –0.2 Pg C (10^{15} g C) in 1987 and 1992, to 0.7 Pg C in 1981 and 1993, because of the combined effects of climate variability and increasing atmospheric CO_2 concentration. A negative NEP means these ecosystems are a source of atmospheric CO_2,

Table 1 Interannual variations in carbon fluxes in Amazonian ecosystems

	Climate with CO_2			Climate only		
Year	NPP (Pg C yr^{-1})	R_H (Pg C yr^{-1})	NEP (Pg C yr^{-1})	NPP (Pg C yr^{-1})	R_H (Pg C yr^{-1})	NEP (Pg C yr^{-1})
1980	5.0	4.7	0.3	4.5	4.5	0.0
1981	5.4	4.7	0.7	4.9	4.4	0.5
1982	4.9	4.8	0.1	4.3	4.5	–0.2
1983	4.8	4.9	–0.1	4.2	4.6	–0.4
1984	5.3	4.8	0.5	4.7	4.5	0.2
1985	5.0	4.8	0.2	4.4	4.4	0.0
1986	5.2	4.8	0.4	4.7	4.5	0.2
1987	4.7	4.9	–0.2	4.1	4.6	–0.5
1988	5.0	4.9	0.1	4.3	4.5	–0.2
1989	5.1	4.8	0.3	4.6	4.5	0.1
1990	5.1	4.8	0.3	4.5	4.5	0.0
1991	4.8	4.9	–0.1	4.1	4.5	–0.4
1992	4.6	4.8	–0.2	3.8	4.4	–0.6
1993	5.7	5.0	0.7	5.1	4.5	0.6
1994	5.3	5.0	0.3	4.7	4.6	0.1
s.d.	0.3	0.1	0.3	0.3	0.1	0.3

The carbon fluxes between the atmosphere and undisturbed Amazonian ecosystems in response to interannual climate variability and increasing atmospheric CO_2 concentration as estimated by the Terrestrial Ecosystem Model. NPP, net primary production; R_H, heterotrophic respiration; NEP, net ecosystem production; s.d., standard deviation. A negative NEP indicates a net flux of carbon from the land to the atmosphere.